Distribution of Measuring Points and Piezoelectric Actuators in Flutter Suppression

CHEN Wei-min[1], GUAN De[2], LI Min[3], ZHU De-chao[2]

(1. Dept. of Mechanics and Engineering Science, Beijing University, Beijing 100871, China)

(2. Dept. of Flight Vehicle Design and Applied Mechanics, Beijing University of Aeronautics and Astronautics, Beijing 100083, China)

(3. The State Key Lab. of Nonlinear Mechanics, Institute of Mechanics of China Science Academy, Beijing 100080, China)

Abstract: Single input/single output (SISO), single input/multi output (SIMO) and multi input/multi output (SIMO) control laws for active flutter suppression are designed and realized in wind tunnel tests. Reasonable agreement between analytical and tested results is achieved. Based on these results, the distribution of response measuring points and piezoelectric actuators is investigated.

Key words: flutter; wind tunnel; piezoelectric

颤振抑制中的测量点和压电驱动器的分布. 陈伟民, 管德, 李敏, 诸德超. 中国航空学报(英文版), 2002, 15(1): 33-37.

摘 要: 对于一个具有分布式压电驱动器的模型, 设计了单输入/单输出(SISO)、单输入/多输出(SIMO)、多输入/多输出(MIMO)颤振主动抑制控制律, 并进行了风洞试验验证。在此基础上, 研究了测量点和压电驱动器的分布。

关键词: 颤振; 风洞试验; 压电

文章编号: 1000-9361(2002)01-0033-05 中图分类号: V214.8 文献标识码: A

The measuring points and actuators should be placed reasonably in flutter suppression using distributed piezoelectric actuators. Three control laws, *i. e.* single input/single output (SISO), single input/multi output (SIMO) and multi input/multi output (MIMO), are designed for the same lifting surface model. Then the wind tunnel test is implemented. Based on the analytical and tested results, the distribution of response measuring points and piezoelectric actuators is investigated.

1 Motion Equation

The model[1] used in this paper is shown in Fig. 1. In areas 1 and 2, piezoelectric actuators are bonded on both sides of an aluminum plate having the same thickness. In order to adjust the flutter velocity to a reasonable level, a lead balance weight is attached in area 3.

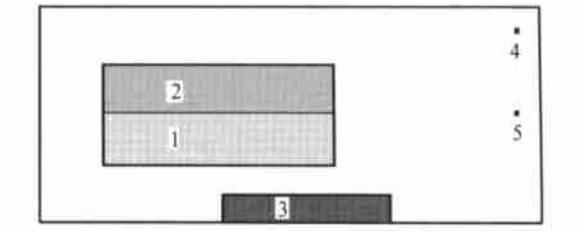

Fig. 1 Plane shape of model

The piezoelectric equation and basic motion equation are similar with those in Ref. [1], so only some results are presented here.

A piezoelectric element is shown in Fig. 2.

The governing equation of motion is presented by means of matrices

$$\boldsymbol{M}\ddot{\xi} + [1 + \mathrm{i}g]\,\omega_n^2 \boldsymbol{M}\xi = \boldsymbol{F}_A + \boldsymbol{F}_V \qquad (1)$$

where ξ is generalized coordinates; displacements $\boldsymbol{w} = \Phi\xi$; Φ is modes shape; and $\boldsymbol{M}$, g, ω_n are generalized mass, structure damping factor and

Received date: 2001-09-07; Revision received date: 2001-11-26
Foundation items: National Nature Science Foundation of China(60034010), and Post Doctor Science Foundation of China
Article URL: http://www.hkxb.net.cn/cja/2002/01/0033/

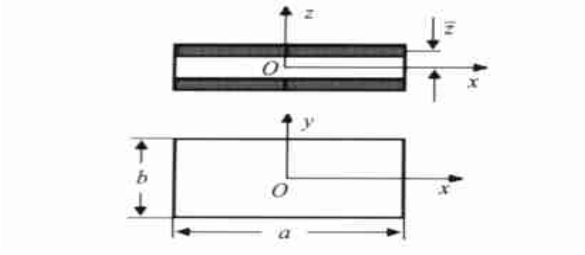

Fig. 2 Piezoelectric element

natural frequency, respectively.

$\boldsymbol{F}_A$ is a generalized aerodynamic force, and $\boldsymbol{F}_A = \frac{1}{2}\rho v^2 \boldsymbol{A}\xi$. Here $\boldsymbol{A}$ is the coefficient matrix of the generalized unsteady aerodynamic force computed out by the subsonic doublet lattice method. ρ, v are free stream density and velocity. The rational function expression of the unsteady aerodynamic force is got by LS method.

$\boldsymbol{F}_V$ is a generalized force due to the external applied electric voltage $\boldsymbol{V}$.

$$\boldsymbol{F}_V = \frac{\boldsymbol{E}_p}{1-\mu} d_{31} \bar{z} \boldsymbol{F} \boldsymbol{V}$$

$$F_{ij} = b \sum_{n=1}^{p_j} \Theta_{xn}^i + a \sum_{n=1}^{p_j} \Theta_{yn}^i \qquad (2)$$

where $\boldsymbol{E}_p$, μ and d_{31} are the Young's modulus, Poisson ratio and piezoelectric constants of the piezoelectric material respectively; $\bar{z}$ is the distance from the mid-plane of the whole laminate plate to the mid-plane of the piezoelectric layer; subscripts, 1, 2, 3, indicate x, y, z directions respectively. b, a, $\bar{z}$ are defined in Fig. 2. Θ is bending angle in mode shape; subscripts, x, y, indicate rotating around x, y axes; p_j is the number of grids of elements in the jth piezoelectric actuator; i denotes the order number of modes.

Introduce a state vector $\boldsymbol{x} = [\xi \quad \dot{\xi} \quad \chi_a]^T$, where χ_a, called aerodynamic generalized vector, is the result of a rational function simulation of the unsteady aerodynamic force. So the state equation is

$$\left.\begin{aligned} \dot{\boldsymbol{x}} &= \boldsymbol{A}\boldsymbol{x} + \boldsymbol{B}\boldsymbol{u} \\ \boldsymbol{y} &= \boldsymbol{C}\boldsymbol{x} \end{aligned}\right\} \qquad (3)$$

where $\boldsymbol{y}$ is the velocity of the measuring point in the z direction.

2 Control Law

SISO, SIMO and MIMO control laws are designed. For SISO, the control voltages applied on actuators 1 and 2 (areas 1 and 2 respectively in Fig. 1) are the same, and point 4 (in Fig. 1) is a measuring point. For SIMO, there are two actuators, actuator 1 and actuator 2, and point 4 (in Fig. 1) is a measuring point too. For MIMO, there are two actuators, actuator 1 and actuator 2, and two measuring points, point 4 and point 5.

Taking account of disturbance on $\boldsymbol{x}$ and $\boldsymbol{y}$, the state equation (3) is expressed as

$$\left.\begin{aligned} \dot{\boldsymbol{x}} &= \boldsymbol{A}\boldsymbol{x} + \boldsymbol{B}\boldsymbol{u} + \Gamma\bar{\boldsymbol{w}} \\ \boldsymbol{y} &= \boldsymbol{C}\boldsymbol{x} + \gamma \end{aligned}\right\} \qquad (4)$$

where $\bar{\boldsymbol{w}}$ and γ are white noise with zero average, whose covariance satisfy

$$E[\bar{\boldsymbol{w}}\bar{\boldsymbol{w}}^T] = Q_f \geqslant 0, \quad E[\gamma\gamma^T] = R_f > 0$$

The feedback $\boldsymbol{u} = -\boldsymbol{K}_0\boldsymbol{x}$ is designed to minimize the performance index

$$J = \int_0^\infty (\boldsymbol{x}^T\boldsymbol{Q}\boldsymbol{x} + \boldsymbol{u}^T\boldsymbol{R}\boldsymbol{u})\,dt$$

where matrix $\boldsymbol{Q}$ is symmetric semi-positive defined and $\boldsymbol{R}$ is symmetric positive defined. So $\boldsymbol{K}_0 = -\boldsymbol{R}^{-1}\cdot\boldsymbol{B}\boldsymbol{P}$.

A Kalman filter is used to estimate the states and the estimated states $\boldsymbol{x}_c$ satisfy

$$\left.\begin{aligned} \dot{\boldsymbol{x}}_c &= \boldsymbol{A}\boldsymbol{x}_c + \boldsymbol{B}\boldsymbol{u} + \boldsymbol{K}_f(\boldsymbol{y} - \boldsymbol{y}_c) \\ \boldsymbol{y}_c &= \boldsymbol{C}\boldsymbol{x}_c \end{aligned}\right\} \qquad (5)$$

where $\boldsymbol{K}_f = \boldsymbol{P}_f\boldsymbol{C}^T\boldsymbol{R}^{-1}$ is feedback gain matrix of the Kalman filter.

$\boldsymbol{P}$ and $\boldsymbol{P}_f$ satisfy different Riccati equations.

In reducing the order of control law, both the balance realization method and LK method are used. In the balance realization method[2], by introducing a transformation, the system would have the same and diagonal observability and controllability Grammian matrices. Then omit those states with weak observability and controllability to reduce the order of the control law.

The LK method[3] distinguishes the states according to their real parts of the eigenroots (latent roots) into "fast" (with high decrement) and

"slow" (with low decrement) modes. Then omit the "fast" mode to reduce the order of the control law.

In the present investigation, the LK method is applied first to omit the states with high decrement, then, the balance realization is used to omit further the states with weak controllability and observability.

Then the control law is transformed into a discrete domain in order to realize the digital control. Tustin transformation is used

3 Tests and Analysis

Through the ground resonance test, the first six order natural frequencies (shown in Table 1) and their mode shapes (node lines are shown in Fig. 3) were obtained. In the ground test, piezoelectric actuators are used as the exciter and the laser vibrameter is used as the sensor to avoid the additional stiffness and mass.

Table 1 Natural frequencies (unit: Hz)

modes	1	2	3	4	5	6
analyzed	3.85	17.40	28.32	53.69	68.47	105.86
tested	3.81	19.44	30.56	63.00	82.50	118.56

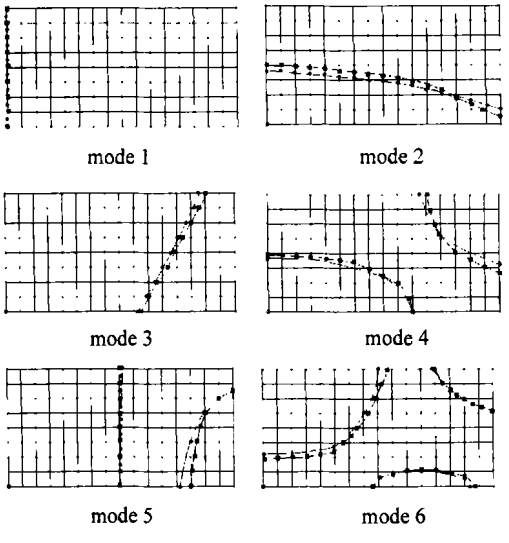

Fig. 3 Node lines of the model

It can be seen from Fig. 3 that the analyzed node lines agree well with the tested ones. Table 1 shows that the analyzed torsion frequencies disagree with the tested ones; according to the results obtained by every test step implemented between manufacturing the models, the disagreement may be mainly due to the trailing edge lead weight, which is not treated in detail in the analytical finite element model. So in the further calculation, the experimental frequencies and calculated modes are used.

Before the wind tunnel test, the control system is tested on the ground. The test sketch is shown in Fig. 4. A typical result (for an example of SIMO) is presented in Fig. 5.

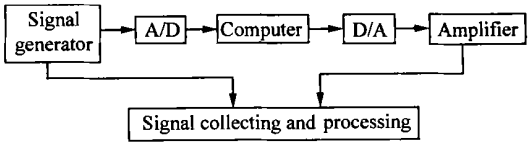

Fig. 4 Ground test of control system

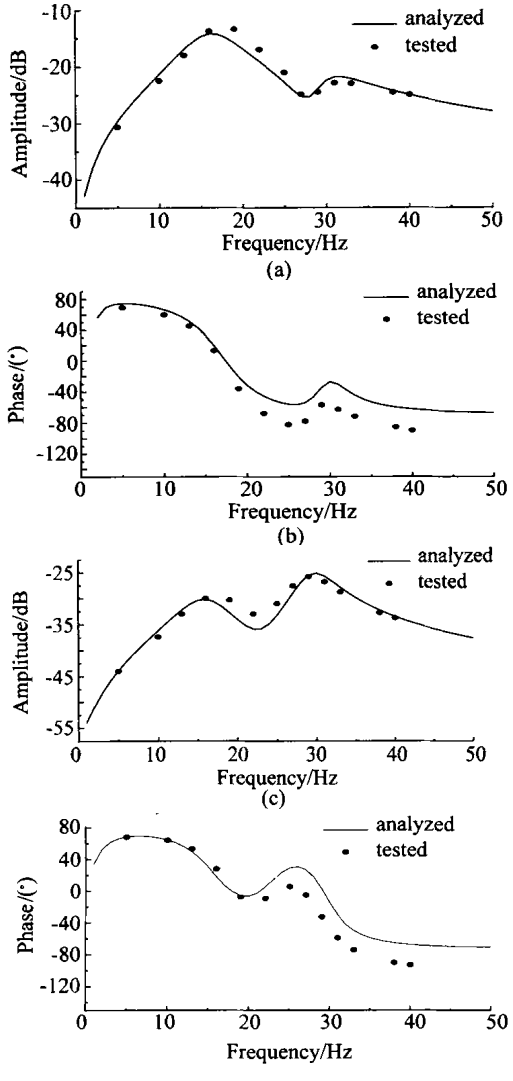

Fig. 5 Results of control system

In Fig. 5, (a) and (b) denote the "amplitude-frequency" and "phase-frequency" curves of the

transformation function of actuator 1 respectively, while (c) and (d) correspond to actuator 2.

Wind tunnel tests were implemented in the open low-speed wind tunnel in Beijing University of Aeronautics and Astronautics. The collocation of MIMO control is shown in Fig. 6.

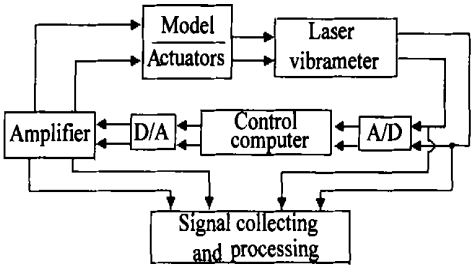

Fig. 6 MIMO wind tunnel test

The flutter velocities and frequencies obtained by analysis and tests are listed in Table 2.

Table 2 Closed loop flutter characters

		Flutter velocity /(m/s)	Flutter frequency /Hz
SISO	Analyzed	31.5	15.1
	Tested	35.3	13.5
SIMO	Analyzed	34.0	14.3
	Tested	33.9	14.0
MIMO	Analyzed	34.0	14.3
	Tested	34.1	14.0

Table 2 states that there is agreement between analyzed and tested flutter characters. Although the tested flutter velocity of SISO is a little higher than the analyzed, tested velocities of SIMO and MIMO agree with analyzed velocities well.

The tested control voltages in subcritical state under three control laws are listed in Table 3. In Table 3 V denotes control voltage; subscripts 1, 2 denote actuator 1 and actuator 2 respectively; SS, SI, MM denote SISO, SIMO, MIMO control law respectively.

Table 3 Control voltage (unit: speed— m/s; voltage— V)

(a) SISO

speed	33.9	35.3
V_{SS}	33.66	58.395

(b) SIMO

speed	30.3	31.8	32.6	33.9
V_{1SM}	9.639	26.265	42.33	52.53
V_{2SM}	2.499	4.335	6.040	9.282

(c) MIMO

speed	28.6	30.0	32.6	33.2	34.1
V_{1MM}	3.876	4.539	39.02	51.51	55.85
V_{2MM}		2.142	5.26	5.61	8.98

Table 3 states that the control voltages, V_{SS}, V_{1SM} and V_{1MM}, at the flutter critical state under three control laws keep the same level. Meanwhile, V_{2SM} is similar with V_{2MM}, and both of them are about 15% of V_{SS}. It proves that the control power under control law SIMO, MIMO, *i.e.* actuator is divided into different groups, and on conditions of similar flutter velocity, is much lower than that of SISO, *i.e.* about 50% of SISO.

It also can be seen in Tables 2, 3 that either the tested flutter characters or the tested control voltages of SIMO and MIMO are similar. So one may say that the measuring point 5 takes a relatively small role.

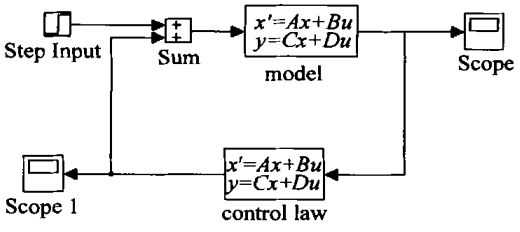

Fig. 7 Sketch of computer simulation

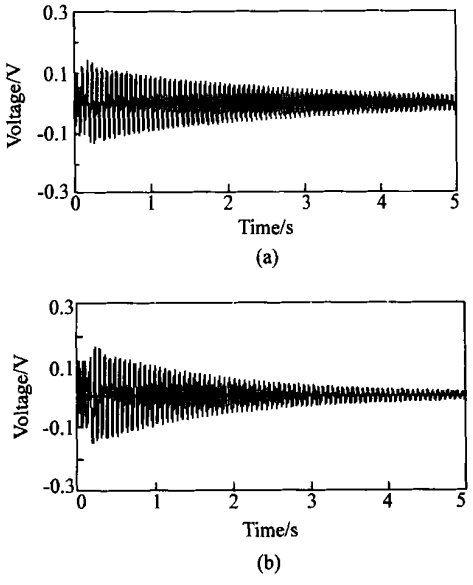

Fig. 8 Simulated control voltage

(a) Using whole actuator; (b) Using a half of actuator

Therefore it is necessary to design a new SISO control law employing actuator 1 and measuring point A. The analyzed flutter velocity is 31.0m/s, which is similar with that of using the whole actuator. In order to compare the control voltage under two SISO control laws, a computer simulation is

performed as shown in Fig. 7. Under the same disturbing and nearing flutter critical point, the control voltages under two SISO control laws are similar (see Fig. 8).

One may say that the results using only a half of the actuators and one measuring point are similar with those of using two actuators and two measuring points.

4 Conclusions

Single input/single output (SISO), single input/multi output (SIMO) and multi input/multi output (SIMO) control laws for active flutter suppression are designed and realized in wind tunnel tests. Reasonable agreement between analytical and tested results is achieved. Based on these results, the distribution of response measuring points and piezoelectric actuators is investigated.

References

[1] GUAN De, CHEN Weimin, LI Min, *et al*. Flutter suppression using distributed piezoelectric actuators[J]. Chinese Journal of Aeronautics, 2000, 13(4): 211– 215.

[2] Moore B C. Principal component analysis in linear system: controllability, observability and model reduction [J]. IEEE Transaction on Automatic Control, 1981, AC-26(1): 17– 31.

[3] Anderson L R. Order reduction of aeroelastic models through LK transformation and riccati iteration[R]. AIAA 93-3795 CP, 1993.

Biographies:

CHEN Weimin Born in 1967, she received Ph. D. degree of aircraft design from Beijing University of Aeronautics and Astronautics in 2000. Her research interests are smart structure and active control. Tel: (010) 82317517

GUAN De Born in 1932, professor and academician, he is devoted to the research of fighter designand aeroelastic mechanics. Tel: (010) 6582 5663

LI Min Born in 1968, he received Ph. D. degree of solid mechanics from Beijing University of Aeronautics and Astronautics in 2000. His research interests are structure dynamic mechanics. Tel: (010) 8231751

ZHU De chao Born in 1933, professor and doctoral supervisor, he is devoted to the research of solid mechanics. Tel: (010) 82317517